ADVANCED HEALTHCARE MATERIALS
www.advhealthmat.de

Influence of Hyaluronan Density on the Behavior of Breast Cancer Cells with Different CD44 Expression

*Ana M. Carvalho, Diana Soares da Costa, Rui L. Reis, and Iva Pashkuleva**

Molecular gradients are common in biosystems and play an essential role in physiological and pathological processes. During carcinogenesis, for example, hyaluronan (HA) homeostasis is dysregulated by cancer cells and the altered synthesis and degradation processes result in the formation of HA gradients within the tumor microenvironment. Herein, a platform is developed to study the biological role of HA gradient in breast cancer cells. Cells with different aggressiveness and expression of CD44—the main HA receptor usually overexpressed in breast cancers, are selected for this study. The developed platform is compatible with several imaging modalities and allows assessment of cell density, morphology, CD44 expression, and cell motility in a function of HA density. Using high-throughput analysis, it is shown that cells that do not express CD44 do not change along the gradient, while CD44 positive cells respond differently to the HA gradient depending on the level of CD44 expression and HA density. This different response is associated with the activation of different signaling pathways by the CD44–HA interactions.

1. Introduction

Cancer development, progression, and recurrence rely on bidirectional communication between cancer cells and the extracellular matrix (ECM).[1] This communication results in ECM remodeling and the formation of both physical and molecular gradients, contributing to a malignant interactome and disease progression.[2] Among different ECM components, hyaluronan (HA)—a linear nonsulfated glycosaminoglycan, is an important player in cancer progression.[1,3] HA synthesis and degradation are tightly regulated, but in most tumors, including breast ones, HA homeostasis is altered, favoring the accumulation of HA fragments and oligosaccharides.[1b,3b,4] The generated fragments modulate the cell behavior of different cell populations within the tumor microenvironment by interaction with HA receptors, including CD44, RHAMM, TLR2/4, and LYVE-1, which activate and/or regulate protumorigenic pathways.[3a] Among these, CD44—a type I transmembrane adhesion glycoprotein, is the main HA receptor commonly upregulated in cancer.[1b,3c,4b,5] CD44/HA interactions are implicated in several signaling cascades toward pathological processes, including cell adhesion, proliferation, cell survival, motility, invasion, and multidrug resistance.[1b,3b,c,6] Moreover, the altered HA turnover also results in the formation of molecular gradients, which might have a pivotal role in tumorigenesis.[2,7]

The experimental setups for elucidation of the HA role in cancer usually rely on supplementation of exogenous HA in solution. Such supplementation differs from the native HA presentation: HA is partially immobilized on the cell surface, where it is secreted by hyaluronan synthases, or in the ECM, where it interacts with other biomolecules.[3b,c] We and others have demonstrated that the presentation of HA affects its bioactivity and signaling.[8] Different immobilization methods that rely on electrostatic interactions, chemical crosslinkers or natural HA binders, e.g., HA-binding proteins and peptides, have been proposed to preserve HA bioactivity in synthetic systems.[8d-g,9] These methods allow the development of systems with customized bioactivity by the use of HA with different molecular weight and degree of modification, i.e., by tailoring the density of the immobilized HA and/or by exposure of epitopes that can be recognized and bind by HA receptors.[8e,9b,d,e,10] Among these different approaches, the immobilization of HA via modification at the reducing end (end-on modification) is of particular interest for biomimicry as it copycats the presentation of HA at the cell surface—it preserves the binding epitopes (no modification along the chain) and allows conformational freedom/flexibility essential for interactions with other biomolecules.[8g,11]

Herein, we developed a 2D platform by end-on immobilization of HA in a continuous gradient fashion. This platform allowed high-throughput screening of cells in contact with the gradients and was validated with two breast cancer cell lines that have different CD44 expression, namely, Sk-Br-3 (CD44−) and MDA-MB-231 (CD44+). These cell lines were characterized in terms of CD44 expression, cell adhesion, morphology, and motility along the HA gradients. Of note, the described platform differs from previously reported HA gradients designed mainly toward investigating the role of stiffness on cell behavior.[12] The development of such bulky (3D) gradients usually requires modification of

A. M. Carvalho, D. Soares da Costa, R. L. Reis, I. Pashkuleva
3B's Research Group - Biomaterials
Biodegradable and Biomimetics
Avepark - Parque de Ciência e Tecnologia Zona Industrial da Gandra
Barco 4805-017, Portugal
E-mail: pashkuleva@i3bs.uminho.pt
A. M. Carvalho, D. Soares da Costa, R. L. Reis, I. Pashkuleva
ICVS/3B's - PT Government Associate Laboratory
University of Minho
Braga/Guimarães Portugal

The ORCID identification number(s) for the author(s) of this article can be found under https://doi.org/10.1002/adhm.202101309

DOI: 10.1002/adhm.202101309

the HA chain (e.g., introducing crosslinkable groups) thus compromising the structure of the native ligand and impeding studies on molecular mechanisms of cellular interactions.

2. Experimental Section

2.1. End-On Modification of Hyaluronan

Sodium hyaluronate (HA, weight average molecular weight (MW) 4.8 kDa, MW dispersity of 1.2) was obtained from Lifecore (USA). HA was modified at the reducing end by oxime reaction with an alkanethiol as previously described.[8a,13] Briefly, HA (200 mg in 5 mL of acetate buffer, pH 4.5) was added to 11-(aminooxy)-1-undecanethiol (3 mol excess to HA) dissolved in 5 mL of ethanol. Aniline (100 µL) was used as a catalyst and added to the reaction mixture. The obtained clear solution was stirred at 45 °C for 24 h. During the reaction, the solution became turbid indicating HA modification. The product was precipitated by adding an excess of ethanol and extensively dialyzed (cut-off 14 kDa, ethanol) to remove any unreacted alkanethiol. Finally, ethanol was evaporated (40 mBar, 50 °C), and the final product was obtained after freeze-drying. The degree of modification was determined by ^{1}H NMR (60 °C in D_2O, Bruker Avance 400 MHz) from the integral's ratio of the peaks corresponding to the aliphatic protons (δ 1.25 ppm) and the proton at C2 of the *N*-acetyl glucosamine unit (δ 3.4 ppm) and calculated to be 98% (Figure S1, Supporting Information).

2.2. Synthesis of Gold Nanoparticles

Gold nanoparticles were synthesized by the Turkevich method as described elsewhere.[14] Briefly, gold (III) chloride trihydrate (95 mL) was heated to 95 °C, and sodium citrate dihydrate (5 mL, i.e., a final concentration of 1×10^{-3} M of gold and 3.8×10^{-3} M of sodium citrate) was added under vigorous magnetic stirring for 15 min. The solution was cooled down to room temperature and stored at 4 °C (stock dispersion). The size of the nanoparticles was determined by atomic force microscopy (AFM; Figure S2B, Supporting Information) and dynamic light scattering (DLS) that showed a diameter of 32 ± 6 nm and 44 ± 1 nm, respectively.

2.3. Preparation of Gradients

Glass coverslips were cleaned with piranha solution and amino-functionalized with 3-(aminopropyl)triethoxysilane (APTES) (details in Supporting Information). Gradients were generated on the aminated coverslips using a two-step procedure. In the first step, a gradient of gold nanoparticles was obtained by diffusional deposition of colloidal nanoparticles. Aminated coverslips were vertically positioned in empty containers, and dispersion of gold nanoparticles (5 mL of the stock dispersion in 95 mL of Milli-Q water) was pumped (100 µL min^{-1}) at the bottom of the container until the coverslips were completely immersed (≈2 h) (**Figure 1**A). The substrates were removed gently from the containers, washed with Milli-Q water, dried under nitrogen flow, and stored at room temperature. The generated gold gradients were characterized by scanning electron microscopy (SEM) and functionalized with HA before each assay. Immobilization of end-on-thiolated HA (500 µg mL^{-1} in Milli-Q water) was carried overnight in an orbital shaker (100 rpm) at room temperature. The substrates were thoroughly washed with NaCl (150×10^{-3} M) and phosphate-buffered saline (PBS) to remove the HA electrostatically deposited on the aminated glass and ensure functionalization only on the gold nanoparticles. The functionalization of the gold gradients with HA and their bioactivity was confirmed by incubation with wheat germ agglutinin (WGA) Alexa Fluor 488 conjugate (1.25 µg mL^{-1} in PBS 10 min) and microscopy imaging (inverted microscope Axio Observer, Zeiss). Before cell studies, surfaces were sterilized by UV light (30 min).

2.4. Culture and Characterization of Breast Cancer Cell Lines

Three breast cancer cell lines were selected for these studies, namely, MDA-MB-231, MDA-MB-468, and Sk-Br-3. However, it was found that MDA-MB-468 cells were CD44+/CD24−, contrary to previous reports that identify these cells as CD44+/CD24+,[15] which is likely caused by genomic instability as indicated by short tandem repeat (STR) DNA profiling (PowerPlex 16 HS System). Therefore, only results about MDA-MB-231 and Sk-Br-3 are presented below. Cells (6×10^4 cells cm^{-2}) were cultured on tissue culture polystyrene using Dulbecco Modified Eagle Medium (DMEM) high glucose with phenol red (Sigma-Aldrich, UK), supplemented with 10% fetal bovine serum (FBS) (Invitrogen, The Netherlands) and 1% antibiotic/antimycotic (Invitrogen, Scotland). Upon 70% of confluence, cells were detached by incubation with 4×10^{-3} M ethylenediaminetetraacetic acid (EDTA, Sigma-Aldrich) in PBS (pH 8, Sigma-Aldrich) for 10 min at 37 °C in 5% CO_2 humidified atmosphere. Cells were characterized by flow cytometry and immunocytochemistry using the following antibodies: human anti-CD44 PE (BD Pharmingen, USA), human anti-CD24 FITC (BD Biosciences, USA), a monoclonal antibody to CD44 - Ascites (Acris, Germany), and AlexaFluor 488 donkey antirabbit IgG (H+L) (Molecular Probes, USA). The expression of surface receptors CD44 and CD24 was quantified by flow cytometry analysis (BD FACSCalibur). Cells were incubated with the respective antibody (anti-CD44-PE or anti-CD24 FITC, 2 µg for 5×10^5 cells in 100 µL of PBS) for 30 min at room temperature, washed with PBS, centrifuged for 5 min at 300 × *g*, and suspended in acquisition buffer (1% formalin in PBS) for analysis. For immunocytochemical characterization, cells were fixed with 10% formalin (4 °C, 1 h) and permeabilized with 0.2% of Triton-X-100/PBS (15 min, room temperature). Incubation with monoclonal antibody to CD44 (dilution 1:400 in 1% BSA/PBS) was performed overnight at 4 °C. After thorough washing with PBS, secondary antibody donkey anti-mouse Alexa Fluor 488 (dilution 1:1000) was added together with DAPI (1 µg mL^{-1}) and phalloidin (0.5 µg mL^{-1}) for nucleus and actin counterstaining (1 h, room temperature). Microscope slides were mounted with VectaShield mounting medium (Vector Laboratories) and observed by an inverted confocal microscope TCS SP8 (Leica Microsystems).

2.5. Interactions of Breast Cancer Cell Lines with the Gradients

Cells were seeded on the gradients at a density of 5×10^4 cells cm^{-2}. For receptor blocking experiments, cells were pretreated with anti-CD44 antibody [KM201] (150 ng mL^{-1} for 1×10^5 cells)

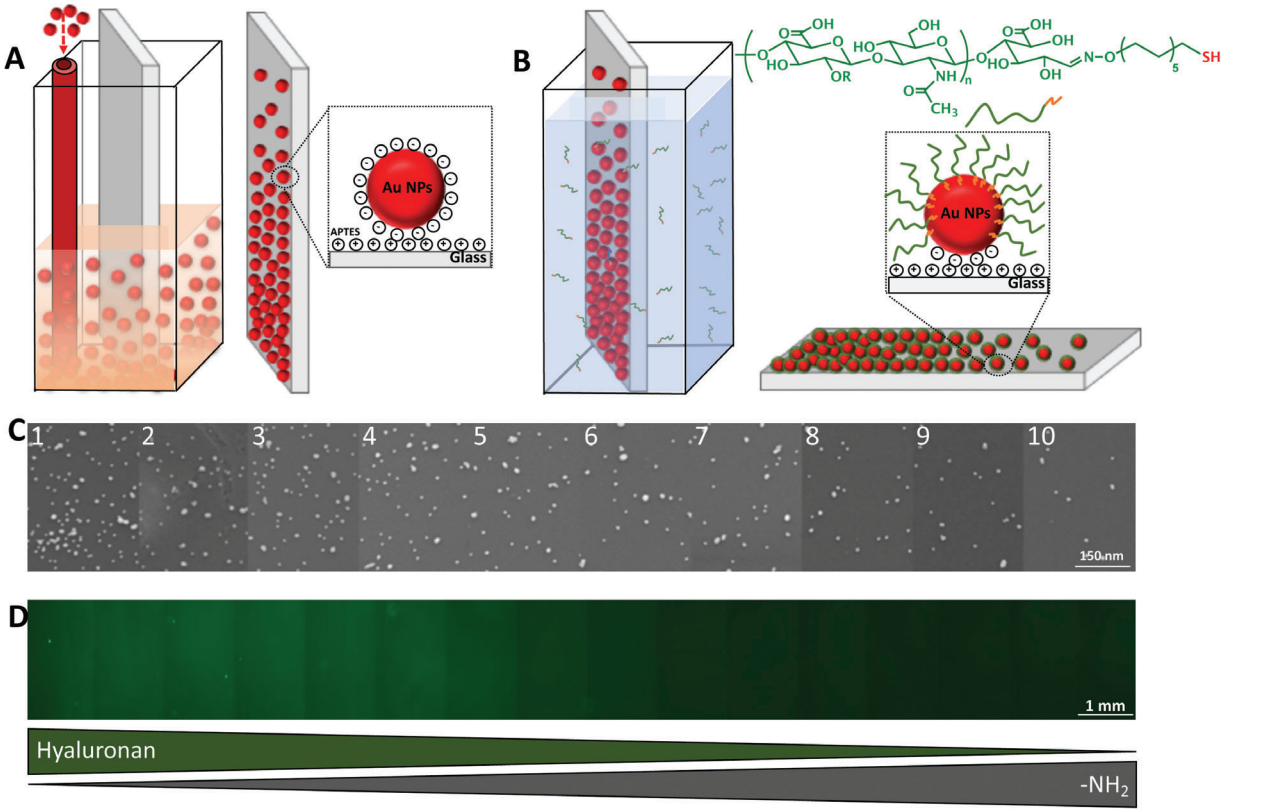

Figure 1. Hyaluronan gradients. Schematic presentation of A) diffusion deposition of gold nanoparticles on aminated glass and B) functionalization of the developed gold nanoparticle gradients with end-on thiolated hyaluronan (HA) to generate the final gradient. C) SEM images of diffusion deposited nanoparticles along the gradients at different equidistant positions. D) Fluorescence tile image of hyaluronan stained with WGA-AlexaFluor 488 conjugate (green). For data analysis, gradients were sectioned in 10 areas, where area 1 corresponds to the bottom of the substrate, i.e., longest contact with colloidal nanoparticles (highest density), and position 10 is at the top of the substrate.

in a complete cell culture medium for 30 min at 37 °C in 5% CO_2 humidified atmosphere and then seeded on the gradients. After 24 h of culture, cells were fixed and characterized by immunocytochemistry and SEM. Immunocytochemistry was performed following the above-described protocol. Tile images of the whole gradient were acquired using an inverted confocal microscope TCS SP8 (Leica Microsystems). Image analysis was performed using Fiji software.[16] To quantify CD44 expression, cells or groups of cells (region of interest) were selected in phalloidin signal (cell body), and the mean gray value of the CD44 channel of each image was determined. Morphometric parameters of individual cells were manually measured in phalloidin signal. The cell aspect ratio was determined with ImageJ, and the cell perimeter to area ratio was calculated from perimeter/area determined with ImageJ. The number of adhered cells was determined by nucleus count.

2.6. SEM

Samples were thoroughly washed with PBS, fixed with 2.5% glutaraldehyde (1 h, 4 °C), dehydrated by incubation in a series of ethanol solutions with increasing concentration (50%, 70%, 90%, and 100%), and dried at room temperature overnight. After mounting on the holders, samples were sputter-coated with gold (1 nm), and images were acquired by high-resolution field emission scanning electron microscope AIRIGA (Zeiss).

2.7. Cell Motility on the Gradients

Cells were cultured on the gradients for 6 h, the medium was removed, and the substrates were washed to remove the nonadherent cells. The adherent cells were followed for 16 h by an inverted optical microscope with incubation (37 °C, 5% CO_2 humidified atmosphere) Axio Observer (Zeiss). Cell tracking was performed using the manual tracking of Fiji software.[16–17] To estimate the cell motility, the traveled distances determined for each timepoint were summed (total distance traveled) and plotted against time.

2.8. Statistical Analysis and Graphical Presentation

All experiments were performed in triplicate ($n = 3$), analyzing at least 2 regions of interest (ROI) per gradient. Data about cellular characteristics as a function of gradient position were graphically presented with the correspondent regression line that showed the respective tendencies in cellular behavior. Data normality and homogeneity of variances were tested by the Shapiro–Wilk normality test and Levene's test for equality of variance, respectively, at

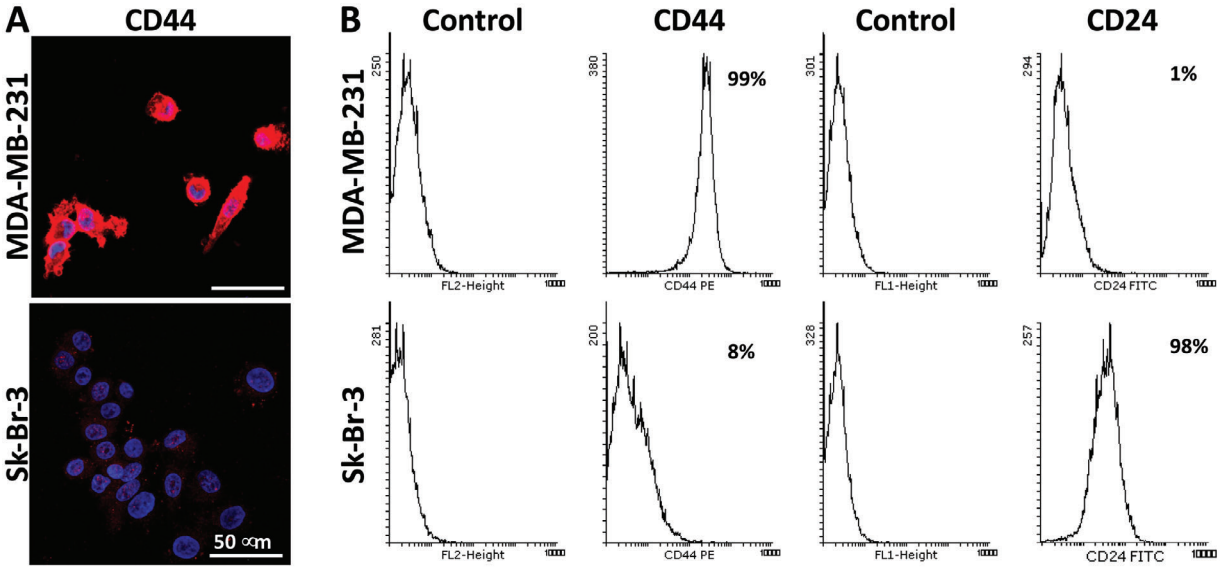

Figure 2. Characterization of breast cancer cell lines MDA-MB-231 and Sk-Br-3. A) Confocal microscopy images of cells stained with DAPI (blue) for nucleus and immunostained for CD44 (red). B) Flow cytometry results showing the surface expression of CD44 and CD24 by the studied cells. Cells were cultured on tissue culture polystyrene for 72 h.

p-value <0.05. Statistical differences among groups (nontreated and CD44 antibody-treated cells) were assessed by the nonparametric Mann–Whitney *U* test with a 95% confidence. Data processing, graphical representation, and statistical analysis were performed using RStudio (Version 1.2.5042).

3. Results and Discussion

3.1. Preparation and Characterization of the Gradients

Biomolecular gradients are essential for life and play a crucial role in physiological and pathological events.[18] As an example, gradients of chemotactic extracellular molecules control all fundamental cellular processes such as survival, signaling, migration, and differentiation. Thus, methods that generate controlled biomolecular gradients present a significant research endeavor. While such bioinspired gradients have different applications (e.g., mimics of the cellular habitat for studying cellular behavior, high-throughput platform for screening ligand expression, biosensing),[19] their development is challenging at different levels. From a biochemical perspective, the difficulties are associated with the demand for a stable immobilization that usually requires biomolecule modification and can compromise its bioactivity.[20] The main obstacles from the fabrication point-of-view are related to the resolution and the gradient size, which must be compatible with the cell size and the targeted application. Usually, nanofabrication methods are applied to fabricate gradients with sufficient resolution (nanoscale), but generally, these methods apply to small substrates. Herein, we developed surface gradients with lenght of 2 cm in two steps (Figure 1).

In the first step, gold nanoparticle gradients were achieved by diffusional deposition of negatively charged gold nanoparticles on positively charged aminated glass (Figure 1A,C). In this method, a longer incubation time leads to a higher density of immobilized gold nanoparticles and allows the formation of continuous linear gradients with high reproducibility between batches (Figure S3, Supporting Information). In the second step, this gradient was functionalized with end-on thiolated HA (Figure 1B). The introduced modification at the reducing end of HA preserves the biofunctionality of this glycosaminoglycan as demonstrated previously.[8a,g,11,13,21] Moreover, such surface presentation of HA is biologically relevant: HA biosynthesis occurs at the cell membrane where hyaluronan synthetases add alternately uridine diphosphate (UDP)-glucuronic acid and UDP-*N*-acetyl glucosamine substrates at the reducing end of the elongating HA chain that is secreted in the pericellular space.[22] The developed gradients have a low gradient slope—properties that allow a high-throughput study of cells behavior in discrete sections (10 positions) and avoid the chemoattractive properties of HA, i.e., a single cell cannot sense (and respond to) the gradient but only to the local concentration of HA at the area on which the cell adheres. Of note, after the HA functionalization, the substrates were not passivated, thus, allowing the formation of a double gradient of HA and $-NH_2$ (Figure 1D) that mimics the competitive and complex cell–ECM interactions (HA-mediated vs non-HA-mediated response).

We used a labeled lectin, namely, WGA that is specific toward *N*-acetyl-D-glucosamine,[23] to confirm the biofunctionality and the resolution of the developed HA gradients (Figure 1D). The results showed that the developed gradients have enough resolution to screen the effect of HA density on cell behavior.

3.2. Characterization of Breast Cancer Cell Lines: CD44 and CD44/CD24 Expression

MDA-MB-231, MDA-MB-468, and Sk-Br-3 breast cancer cell lines were chosen for this study based on previous data for their different CD44 expression and aggressiveness. Fluorescence microscopy and flow cytometry analysis (**Figure 2**) confirmed that

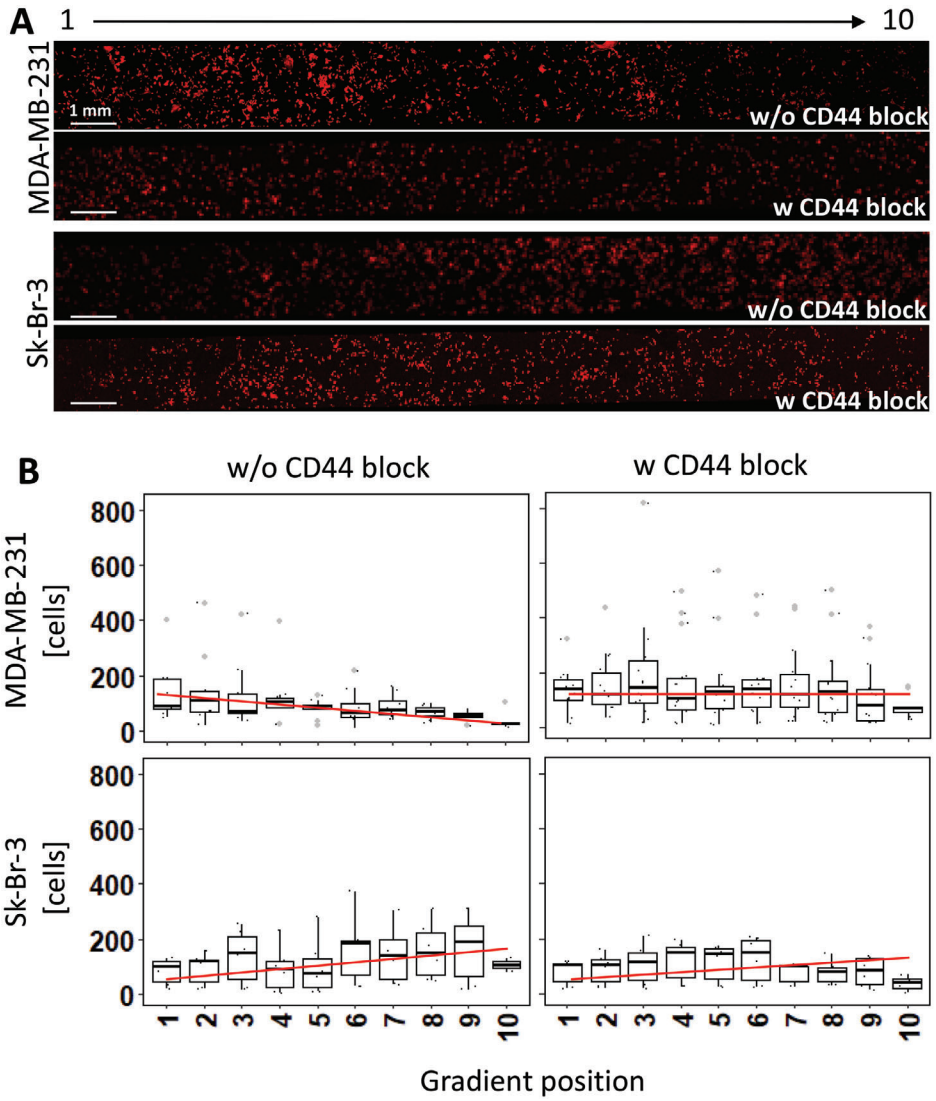

Figure 3. Cell adhesion on HA gradients. A) Representative tile images of MDA-MB-231 and Sk-Br-3 cells cultured on HA gradients for 24 h. B) Distribution of the adherent cells along the gradients (outliers are presented in gray). In the two experimental sets, we used cells without (w/o) and with (w) previous treatment with function-blocking antibody to CD44 (CD44 block). Cells' actin cytoskeleton was stained with phalloidin (red). Significant differences were observed between MDA-MD-231 cells seeded on HA gradients and controls (gold gradients, $p < 0.01$) and between MDA-MD-231 cells w/o and w CD44 block ($p < 0.001$). In the graphs, HA density decreases from position 1 to position 10.

MDA-MB-231 and MDA-MB-468 (data not shown) cells were CD44+ (mean fluorescence intensity determined by flow cytometry MFI (MDA-MB-231) = 233). On the other hand, Sk-Br-3 cells were CD44− (Figure 2). The surface expression of CD44 is related to cancer aggressiveness and stemness: CD44+/CD24− cells are more aggressive than other phenotypes.[15,24] In conformity with these previous reports, our flow cytometry data (Figure 2B) showed that MDA-MB-231 cells have CD44+/CD24− phenotype (MFI CD44/CD24 was 11.41 ± 1.52), while Sk-Br-3 cells are CD44−/CD24+ (MFI CD44/CD24 = 0.59 ± 0.12), confirming different degrees of aggressiveness.[15] Surprisingly, MDA-MB-468 cells were CD44+/CD24+, which is against previous data for this cell line identifying them as CD44+/CD24−.[15] Further analysis of these cells by STR DNA profiling showed more alleles than the ones reported in the databases, indicating genetic instability. Thus, the data generated with this cell line are not shown.

3.3. Cell Adhesion on the HA Gradients

MDA-MB-231 and Sk-Br-3 cells were differently distributed along the gradients (**Figure 3**). The influence of the HA density on the adhesion of MDA-MB-231 cells was evident: the number of adherent cells raised progressively along the gradient with increasing HA density, reaching maximum values at position 1, i.e., at the highest HA density.

In the case of Sk-Br-3 cells, the trend was opposite—fewer adherent cells were observed at high HA density (Figure 3B). To check whether this response is driven by the recognition of

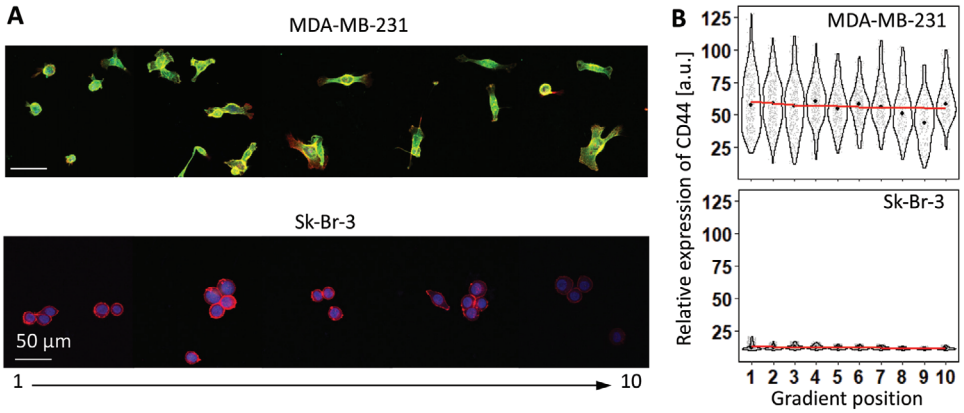

Figure 4. Expression of CD44 by breast cancer cells adhered on the HA gradients. A) Representative fluorescence images and B) graphical presentation showing the expression of CD44 by MDA-MB-231 and Sk-Br-3 cells along the gradient. Nuclei are stained in blue, the actin cytoskeleton in red, and CD44 in green. In the graphs, gray points represent each measurement of CD44 expression, and red dots represent the median value for each position. HA density decreases from 1 to 10. Data for control substrates (gradients without HA functionalization) are presented in Figure S4 in the Supporting Information. CD44 expression by MDA-MB-231 cells was significantly different ($p < 0.0001$) from the CD44 expression by Sk-Br-3 cells at all studied conditions. The expression of CD44 by cells seeded on control gradients was significantly different ($p < 0.0001$) by the CD44 expression on HA gradients for both cell lines.

HA on the surface, we treated the cells with a function-blocking antibody for CD44 before seeding on the gradients.[8b] This treatment changed the adhesion trend for the MDA-MB-231 cells: we observed homogeneously distributed cells along the gradient. CD44 blocking did not have such an effect on Sk-Br-3 cells that maintain their profile. These results indicated different adhesion mechanisms for the studied cell lines. The adhesion of MDA-MB-231 to the gradients is HA-dependent and mediated by CD44. Sk-Br-3 are CD44− and other receptors, most probably syndecans, mediate their adhesion as the number of adherent cells increases with the augmentation of the $-NH_2$ density (opposite to HA density).

3.4. Expression of CD44 as a Function of HA Gradient

In breast cancer, changes in HA metabolism are observed since the early stages: the high HA content in the pericellular space and ECM provides adhesion points and activates signaling cascades toward cell growth and proliferation, which are critical for tumorigenesis processes.[3a,25] CD44 is involved in most of these processes: it is commonly overexpressed in breast cancer and thus it is a therapeutic target.[4b,5a] We assessed the CD44 expression by the adherent cells along the gradients (**Figure 4**). Similar CD44 expression (low and no differences along the gradient) was determined for both studied cell lines on the control substrates—gradients without HA (Figure S4, Supporting Information). Functionalization of the gradients with HA increased significantly the expression of CD44 by MDA-MB-231 cells (CD44+), while Sk-Br-3 cells (CD44−) maintained an expression profile similar to the control gradients. These results are consistent with previous studies reporting feedback response upon HA binding that regulates CD44 expression[6b,8a] and show that this feedback depends on the HA presence and cell phenotype. Dysregulated HA homeostasis and consequent HA accumulation in the pericellular space at the early cancer stage is crucial for recruiting cells and activating protumorigenic pathways related with enhanced proliferation, motility, apoptosis, and drug resistance.[1b,3b,c,6] Additionally, the induced high expression of CD44 is recognized as a marker of cancer cell stemness, and its interaction with HA activates stemness-related pathways resulting in tumor recurrence.[26]

3.5. Cell Morphology on HA Gradient

Because some studies have reported CD44 as a cytoskeletal regulator that influences cell morphology upon interaction with HA,[6b] we also assessed morphological changes along the gradients. We determined the cell aspect ratio and cell perimeter to surface area ratio for the studied cell lines (**Figure 5**). We did not find any effect of HA density on the cells' aspect ratio (Figure S5, Supporting Information). Cell perimeter to surface area ratio can be used as an indicator for the formation of cellular protrusions, e.g., lamellipodia and filopodia (Figure 5A).[27]

We did not observe morphological changes for MDA-MB-231 cells along the HA gradient. Nevertheless, confocal images of these cells show an increase of cell spreading along HA gradient, which is consistent with the adhesive phenotype driven by CD44 expression. The morphology of CD44− Sk-Br-3 cells did not change along the gradient and the parameters were similar for HA-functionalized gradients and control (Figure 5B vs Figure S5B in the Supporting Information).

SEM images (Figure 5C,D; Figure S8, Supporting Information) corroborated the morphology differences between CD44+ and CD44− cells: filopodia are the main adhesion structures observed in MDA-MB-231 cells, while Sk-Br-3 cells interact with the surface mainly by lamellipodia and only a few short filopodia are present at the edge of the cells. Importantly, filopodia interact with HA-functionalized spots on the gradients (**Figure 6**): confocal orthogonal views of cell protrusions showed colocalization of CD44, actin, and gold for the filopodia of MDA-MB-231 cells. In the case of the Sk-Br-3 lamellipodia, we observed colocalization of actin and gold only. These results corroborate previous reports

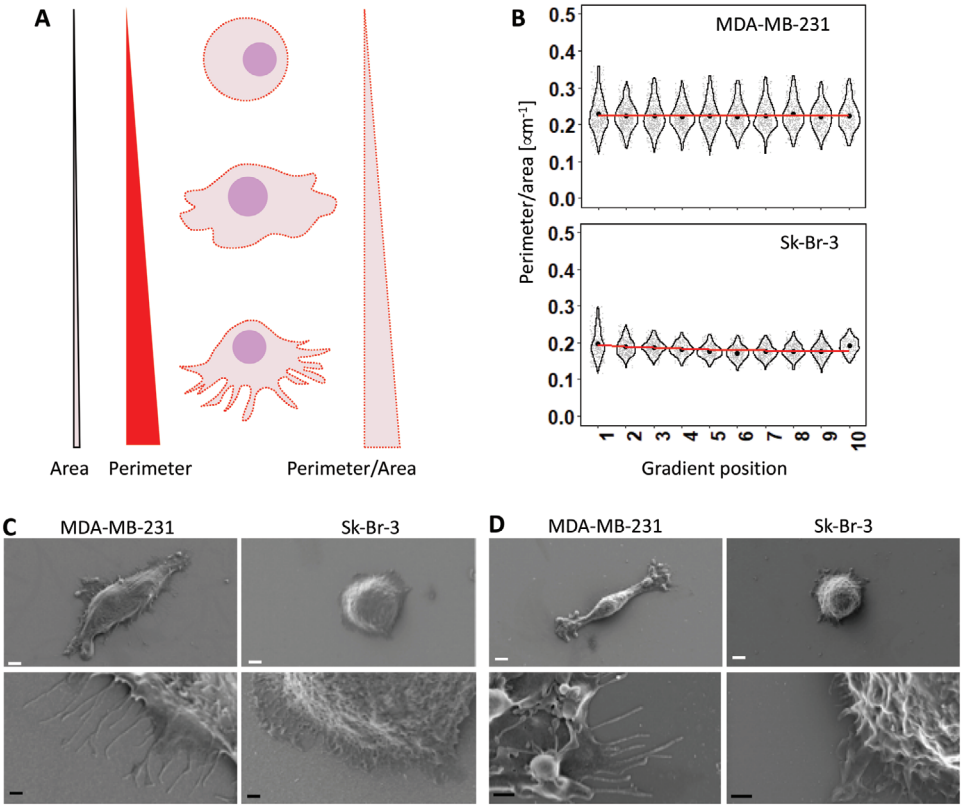

Figure 5. Morphology of breast cancer cell lines interacting with the HA gradients. A) Schematic presentation of the morphological parameters used for the analysis. B) Cell perimeter to surface area ratio for MDA-MB-231 and Sk-Br-3 cells cultured on the gradients for 24 h. Representative scanning electron microscopy images of the studied cell lines at C) position 1 and D) position 10 of the gradients (white scale bar = 4 µm; black scale bar = 1 µm). Cell aspect ratio and surface area of MDA-MB-231 cells were significantly different ($p < 0.0001$) from the parameters determined for Sk-Br-3 cells at all studied conditions. Data for cell aspect ratio (Figure S5, Supporting Information), cells on control substrates (Figure S6, Supporting Information), and additional SEM images (Figures S7 and S8, Supporting Information) are provided.

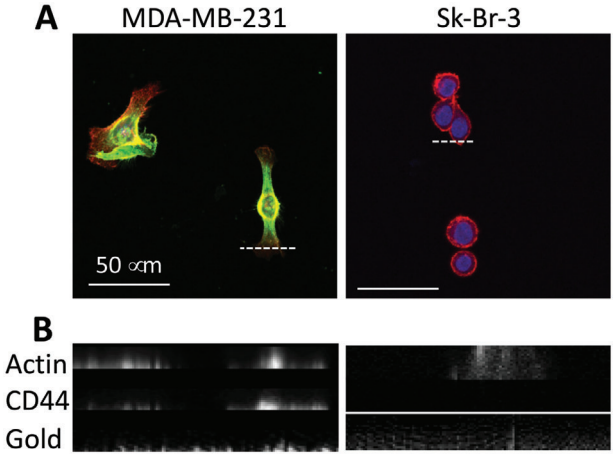

Figure 6. Colocalization of actin (red), CD44 (green), and gold for the studied cell lines: A) Maximum projections (z-stacks) and B) orthogonal YZ confocal microscopy images of cell protrusions (filopodia of MDA-MB-231 cells and lamellipodia of Sk-Br-3 cells). Analyzed sections are shown by dashed lines.

on the role of CD44–HA interactions in the formation and lengthening of filopodia processes, promoting cell migration.[28]

3.6. Cells Motility on HA Gradient

MDA-MB-231 and Sk-Br-3 have different aggressive phenotypes, and thus, we have also studied the effect of HA density on cell motility (**Figure 7**). We observed random cell migration for the studied cell lines but their motility was different: significantly ($p < 0.0001$) longer distance traveled was determined for MDA-MB-231 cells than for Sk-Br-3 cells (Figure 7A). Moreover, MDA-MB-231 cells showed increased motility at higher HA density, while similar values were observed for Sk-Br-3 cells along the HA gradient.

These results agree with the performed characterization of the cell lines (Figure 2) and the literature that reports high aggressiveness[8a,15,24] and metastatic potential for MDA-MB-231 cells upon their interaction with ECM components, including immobilized HA.[29] Moreover, CD44 blocking reduced the total traveled distance of MDA-MB-231 cells on the gradients significantly (Figure 7B), confirming that CD44–HA interactions are involved in the signaling cascade of MDA-MB-231 motility. Sk-Br-3 cells traveled shorter distances than those measured for

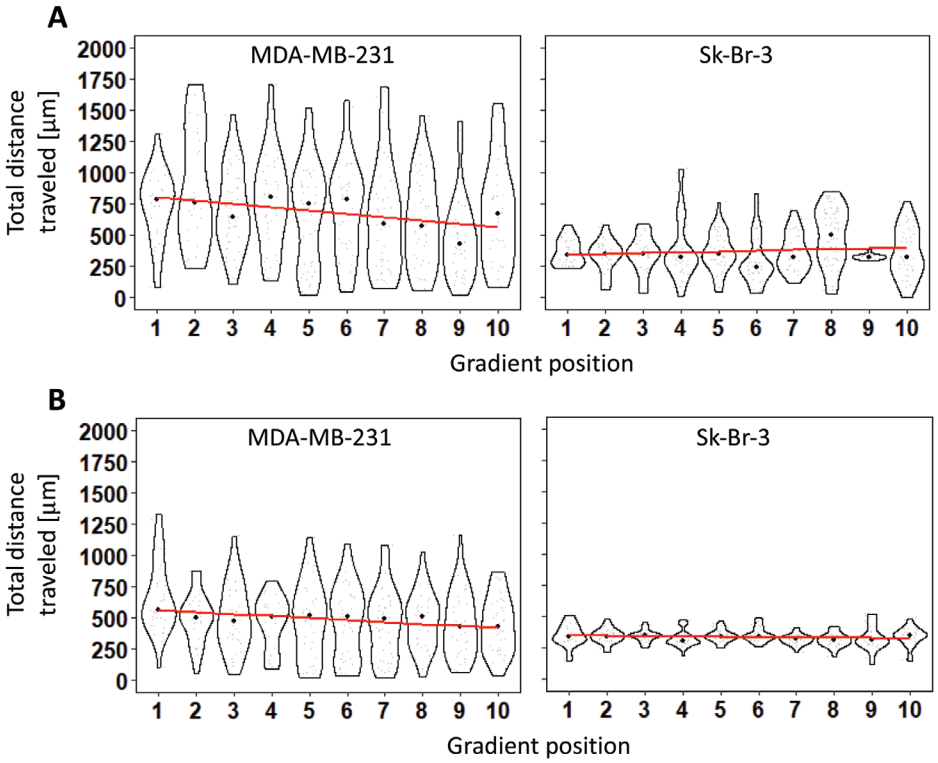

Figure 7. Breast cancer cell motility on the gradients: Total distance traveled of MDA-MB-231 and Sk-Br-3 cells A) without and B) with CD44 blocking.

MDA-MB-231 and did not change along the gradients. When we blocked the CD44 in these cells, we observed no significant differences in cell motility for Sk-Br-3 cells along the gradient (Figure 7B).

4. Conclusions

We developed a platform that allows the presentation of HA in a biorelevant manner and in a gradient fashion and is also compatible with several high-throughput characterization methods. Our results demonstrated that this platform is a valuable tool for studying cell behavior in response to HA density. We showed that CD44/HA interactions result in different cell response associated with cell phenotype and HA density, thus, highlighting the importance of bidirectional communication between cell traits and ECM. At higher HA density, we observed an increased cell density and motility for the CD44+ MDA-MB-231 cells when compared to the CD44− Sk-Br-3 cells. These responses agree with the different aggressive phenotypes of these cells and suggest that HA/CD44 interactions have different roles at different cancer stages. Treatment with function-blocking antibody to CD44 receptor inhibited the cells' response to HA density, showing the potential of the developed platform in screening possible blockers, competitors, and inhibitors of cell-HA interactions in diverse diseases.

Supporting Information

Supporting Information is available from the Wiley Online Library or from the author.

Acknowledgements

The authors thank the Portuguese FCT (Grants Nos: SFRH/BD/114 847/2016 and PTDC/NAN-MAT/28 468/2017) and EU (Grant No: 668983-Forecast) for providing financial support to this project.

Conflict of Interest

The authors declare no conflict of interest.

Data Availability Statement

Data sharing is not applicable to this article as no new data were created or analyzed in this study.

Keywords

biomolecular gradients, breast cancer, CD44, high-throughput platforms, hyaluronic acid

Received: July 2, 2021
Revised: October 18, 2021
Published online:

[1] a) T. R. Cox, *Nat. Rev. Cancer* **2021**, *21*, 217; b) J. Winkler, A. Abisoye-Ogunniyan, K. J. Metcalf, Z. Werb, *Nat. Commun.* **2020**, *11*, 5120.
[2] M. J. Oudin, V. M. Weaver, *Cold Spring Harbor Symp. Quant. Biol.* **2016**, *81*, 189.

[3] a) I. Caon, B. Bartolini, A. Parnigoni, E. Carava, P. Moretto, M. Viola, E. Karousou, D. Vigetti, A. Passi, *Semin. Cancer Biol.* **2020**, *62*, 9; b) B. P. Toole, *Nat. Rev. Cancer* **2004**, *4*, 528; c) E. A. Turley, D. K. Wood, J. B. McCarthy, *Cancer Res.* **2016**, *76*, 2507.
[4] a) P. Heldin, K. Basu, B. Olofsson, H. Porsch, I. Kozlova, K. Kahata, *J. Biochem.* **2013**, *154*, 395; b) P. Auvinen, R. Tammi, J. Parkkinen, M. Tammi, U. Agren, R. Johansson, P. Hirvikoski, M. Eskelinen, V. M. Kosma, *Am. J. Pathol.* **2000**, *156*, 529.
[5] a) X. Liu, R. Taftaf, M. Kawaguchi, Y.-F. Chang, W. Chen, D. Entenberg, Y. Zhang, L. Gerratana, S. Huang, D. B. Patel, *Cancer Discovery* **2019**, *9*, 96; b) C. Chen, S. Zhao, A. Karnad, J. W. Freeman, *J. Hematol. Oncol.* **2018**, *11*, 64.
[6] a) L. Y. Bourguignon, M. Shiina, J.-J. Li, *Adv. Cancer Res.* **2014**, *123*, 255; b) M. Zoller, *Nat. Rev. Cancer* **2011**, *11*, 254.
[7] a) H. Boehm, T. A. Mundinger, C. H. J. Boehm, V. Hagel, U. Rauch, J. P. Spatz, J. E. Curtis, *Soft Matter* **2009**, *5*, 4331; b) G. Tzircotis, R. F. Thorne, C. M. Isacke, *J. Cell Sci.* **2005**, *118*, 5119.
[8] a) A. M. Carvalho, D. S. da Costa, P. M. R. Paulo, R. L. Reis, I. Pashkuleva, *Acta Biomater.* **2021**, *119*, 114; b) S. Amorim, D. S. da Costa, D. Freitas, C. A. Reis, R. L. Reis, I. Pashkuleva, R. A. Pires, *Sci. Rep.* **2018**, *8*, 16058; c) J. Sapudom, F. Ullm, S. Martin, L. Kalbitzer, J. Naab, S. Moller, M. Schnabelrauch, U. Anderegg, S. Schmidt, T. Pompe, *Acta Biomater.* **2017**, *50*, 259; d) A. Herrera-Gayol, S. Jothy, *Int. J. Exp. Pathol.* **2001**, *82*, 193; e) A. Almalik, S. Karimi, S. Ouasti, R. Donno, C. Wandrey, P. J. Day, N. Tirelli, *Biomaterials* **2013**, *34*, 5369; f) H. H. Duan, M. Donovan, F. Hernandez, C. Di Primo, E. Garanger, X. Schultze, S. Lecommandoux, *Angew. Chem., Int. Ed.* **2020**, *59*, 13591; g) N. Altgärde, E. Nilebäck, L. de Battice, I. Pashkuleva, R. L. Reis, J. Becher, S. Möller, M. Schnabelrauch, S. Svedhem, *Acta Biomater.* **2013**, *9*, 8158.
[9] a) H. AlKhoury, A. Hautmann, F. Erdmann, G. Y. Zhou, S. Stojanovic, S. Najman, T. Groth, *J. Biomed. Mater. Res., Part A* **2020**, *108*, 1099; b) G. L. Zhang, Y. Q. He, Y. W. Liu, Y. Du, C. X. Yang, F. Gao, *Cell Death Dis.* **2021**, *12*, 586; c) X. Q. Pang, W. Q. Li, L. Chang, J. E. Gautrot, W. Wang, H. S. Azevedo, *ACS Appl. Mater. Interfaces* **2021**, *13*, 25792; d) N. S. Baranova, E. Nileback, F. M. Haller, D. C. Briggs, S. Svedhem, A. J. Day, R. P. Richter, *J. Biol. Chem.* **2011**, *286*, 25675; e) S. Amorim, I. Pashkuleva, C. A. Reis, R. L. Reis, R. A. Pires, *J. Mater. Chem. B* **2020**, *8*, 3880.
[10] S. Mizrahy, S. R. Raz, M. Hasgaard, H. Liu, N. Soffer-Tsur, K. Cohen, R. Dvash, D. Landsman-Milo, M. G. E. G. Bremer, S. M. Moghimi, D. Peer, *J. Controlled Release* **2011**, *156*, 231.
[11] P. M. Wolny, S. Banerji, C. Gounou, A. R. Brisson, A. J. Day, D. G. Jackson, R. P. Richter, *J. Biol. Chem.* **2010**, *285*, 30170.
[12] a) S. H. Oh, D. B. An, T. H. Kim, J. H. Lee, *Acta Biomater.* **2016**, *35*, 23; b) S. L. Vega, M. Y. Kwon, K. H. Song, C. Wang, R. L. Mauck, L. Han, J. A. Burdick, *Nat. Commun.* **2018**, *9*, 614; c) A. D. Rape, M. Zibinsky, N. Murthy, S. Kumar, *Nat. Commun.* **2015**, *6*, 8129.
[13] A. M. Carvalho, R. Teixeira, R. Novoa-Carballal, R. A. Pires, R. L. Reis, I. Pashkuleva, *Biomacromolecules* **2018**, *19*, 2991.
[14] J. Kimling, M. Maier, B. Okenve, V. Kotaidis, H. Ballot, A. Plech, *J. Phys. Chem. B* **2006**, *110*, 15700.
[15] W. Li, H. Ma, J. Zhang, L. Zhu, C. Wang, Y. Yang, *Sci. Rep.* **2017**, *7*, 13856.
[16] J. Schindelin, I. Arganda-Carreras, E. Frise, V. Kaynig, M. Longair, T. Pietzsch, S. Preibisch, C. Rueden, S. Saalfeld, B. Schmid, J.-Y. Tinevez, D. J. White, V. Hartenstein, K. Eliceiri, P. Tomancak, A. Cardona, *Nat. Methods* **2012**, *9*, 676.
[17] E. Meijering, O. Dzyubachyk, I. Smal, *Methods Enzymol.* **2012**, *504*, 183.
[18] a) D. Ellison, A. Mugler, M. D. Brennan, S. H. Lee, R. J. Huebner, E. R. Shamir, L. A. Woo, J. Kim, P. Amar, I. Nemenman, *Proc. Natl. Acad. Sci. USA* **2016**, *113*, E679; b) J. Gurdon, S. Dyson, D. St Johnston, *Cell* **1998**, *95*, 159.
[19] a) S. Morgenthaler, C. Zink, N. D. Spencer, *Soft Matter* **2008**, *4*, 419; b) M. Riepl, M. Östblom, I. Lundström, S. C. Svensson, A. W. Denier van der Gon, M. Schäferling, B. Liedberg, *Langmuir* **2005**, *21*, 1042; c) A. Lagunas, E. Martínez, J. Samitier, *Front. Bioeng. Biotechnol.* **2015**, *3*, 132.
[20] I. Pashkuleva, R. L. Reis, *J. Mater. Chem.* **2010**, *20*, 8803.
[21] N. Tanaka, Y. Yoshiike, C. Yoshiyama, T. Kitaoka, *Carbohydr. Polym.* **2010**, *82*, 100.
[22] R. H. Tammi, A. G. Passi, K. Rilla, E. Karousou, D. Vigetti, K. Makkonen, M. I. Tammi, *FEBS J.* **2011**, *278*, 1419.
[23] M. Monsigny, A. C. Roche, C. Sene, R. Maget-Dana, F. Delmotte, *Eur. J. Biochem.* **1980**, *104*, 147.
[24] A. Jaggupilli, E. Elkord, *Clin. Dev. Immunol.* **2012**, *2012*, 708036.
[25] M. Liu, C. Tolg, E. Turley, *Front. Immunol.* **2019**, *10*, 947.
[26] T. Kashyap, K. K. Pramanik, N. Nath, P. Mishra, A. K. Singh, S. Nagini, A. Rana, R. Mishra, *Oral Oncol.* **2018**, *86*, 234.
[27] M. R. Mejillano, S.-i. Kojima, D. A. Applewhite, F. B. Gertler, T. M. Svitkina, G. G. Borisy, *Cell* **2004**, *118*, 363.
[28] a) A. Pusch, A. Boeckenhoff, T. Glaser, T. Kaminski, G. Kirfel, M. Hans, B. Steinfarz, D. Swandulla, U. Kubitscheck, V. Gieselmann, *Biochim. Biophys. Acta, Mol. Cell Res.* **2010**, *1803*, 261; b) K. N. Sugahara, T. Murai, H. Nishinakamura, H. Kawashima, H. Saya, M. Miyasaka, *J. Biol. Chem.* **2003**, *278*, 32259; c) K. Härkönen, S. Oikari, H. Kyykallio, J. Capra, S. Hakkola, K. Ketola, U. Thanigai Arasu, G. Daaboul, A. Malloy, C. Oliveira, *Cells* **2019**, *8*, 276; d) S. Twarock, M. I. Tammi, R. C. Savani, J. W. Fischer, *J. Biol. Chem.* **2010**, *285*, 23276.
[29] A. Köwitsch, A. Chhalotre, T. Groth, *J. Artif. Organs* **2017**, *40*, 31.